

# Highly efficient THz generation by optical rectification of mid-IR pulses in DAST

Cite as: APL Photonics 6, 046105 (2021); <https://doi.org/10.1063/5.0037235>

Submitted: 11 November 2020 . Accepted: 28 March 2021 . Published Online: 22 April 2021

 Claudia Gollner, Mostafa Shalaby, Corinne Brodeur,  Ignas Astrauskas, Rokas Jutas, Evan Constable, Lorenz Bergen, Andrius Baltuška, and  Audrius Pugžlys



View Online



Export Citation



CrossMark

## ARTICLES YOU MAY BE INTERESTED IN

[New perspective on chiral exceptional points with application to discrete photonics](#)

APL Photonics 6, 040803 (2021); <https://doi.org/10.1063/5.0045459>

[Terahertz optical machine learning for object recognition](#)

APL Photonics 5, 126103 (2020); <https://doi.org/10.1063/5.0029310>

[Spintronic terahertz emitter](#)

Journal of Applied Physics 129, 010901 (2021); <https://doi.org/10.1063/5.0037937>

APL Photonics

SPECIAL TOPIC: Perovskite Photonics

# Highly efficient THz generation by optical rectification of mid-IR pulses in DAST

Cite as: APL Photon. 6, 046105 (2021); doi: 10.1063/5.0037235  
Submitted: 11 November 2020 • Accepted: 28 March 2021 •  
Published Online: 22 April 2021



Claudia Gollner,<sup>1</sup> Mostafa Shalaby,<sup>2,3</sup> Corinne Brodeur,<sup>2</sup> Ignas Astrauskas,<sup>1</sup> Rokas Jutas,<sup>4</sup>  
Evan Constable,<sup>5</sup> Lorenz Bergen,<sup>5</sup> Andrius Baltuška,<sup>1,6</sup> and Audrius Pugžlys<sup>1,6,a)</sup>

## AFFILIATIONS

<sup>1</sup> Photonics Institute, TU Wien, Gusshausstrasse 27-387, A-1040 Vienna, Austria

<sup>2</sup> Swiss Terahertz Research-Zurich, Techpark, 8005 Zurich, Switzerland and Park Innovaare, 5234 Villigen, Switzerland

<sup>3</sup> Key Laboratory of Terahertz Optoelectronics, Beijing Advanced Innovation Center for Imaging Technology CNU, Beijing 100048, China

<sup>4</sup> Institute of Control Systems (IRS), Karlsruhe Institute of Technology (KIT), Kaiserstr. 12, 76131 Karlsruhe, Germany

<sup>5</sup> Institute of Solid State Physics, TU Wien, 1040 Vienna, Austria

<sup>6</sup> Center for Physical Sciences and Technology, Savanoriu Ave. 231, LT-02300 Vilnius, Lithuania

<sup>a)</sup> Author to whom correspondence should be addressed: [audrius.pugzlys@tuwien.ac.at](mailto:audrius.pugzlys@tuwien.ac.at)

## ABSTRACT

We report on efficient THz generation in DAST by optical rectification of intense mid-IR pulses centered at (i)  $3.9\ \mu\text{m}$  and (ii) its second harmonic at  $1.95\ \mu\text{m}$ . Suppression of multi-photon absorption shifts the onset of saturation of the THz conversion efficiency to pump energy densities, which are almost an order of magnitude higher as compared to conventional pump schemes at  $1.5\ \mu\text{m}$ . Despite strong linear absorption at  $3.9\ \mu\text{m}$ , DAST exhibits a high optical-to-THz conversion efficiency, which we attribute to resonantly enhanced nonlinearity and advantageous phase matching of the THz phase velocity and group velocity of the driving pulse. At  $1.95\ \mu\text{m}$ , we find that low linear and multi-photon absorption in combination with cascaded optical rectification lead to record optical-to-THz conversion efficiencies approaching 6%. The observed high sensitivity of the THz generation to the parameters of the mid-IR driving pulses motivates an in-depth study of the underlying interplay of nonlinear wavelength- and intensity-dependent effects.

© 2021 Author(s). All article content, except where otherwise noted, is licensed under a Creative Commons Attribution (CC BY) license (<http://creativecommons.org/licenses/by/4.0/>). <https://doi.org/10.1063/5.0037235>

## I. INTRODUCTION

Within the last few decades, terahertz spectroscopy,<sup>1-3</sup> where the THz pulse mainly acts as a linear probe, has become a versatile tool to explore a multitude of physical phenomena by probing low-energy transitions situated in the THz range, governed by phonon-, plasmon-, and spin-resonances; intersubband passages; excitons; or molecular rotations.<sup>4,5</sup> Intense terahertz (THz) pulses with an electric field strength exceeding the intrinsic field of atoms have large potential to engineer new dynamic states in a wide range of materials. In recent years, trend-setting experiments, wherein the THz pulse acts as a non-linear (NL) pump, have been demanding intense, broadband THz sources.<sup>6-8</sup> This exciting new research area provides an opportunity to control matter by coherent lattice excitation, to trigger transient phase transitions and engineer new dynamic states

of materials,<sup>9</sup> such as THz enhanced superconductivity,<sup>10</sup> polarization switching in ferroelectric materials,<sup>11</sup> or ultrafast switching and controlling of magnetic domains.<sup>12</sup>

Currently, increasingly promising tabletop sources for THz generation are based on optical rectification (OR) of fs-pulses in electro-optic crystals (EOCs). Recently, considerable progress has been achieved with organic crystals, such as DAST (4-N,N-dimethylamino-4'-N'-methylstilbazolium tosylate) and its derivative DSTMS (4-N,N-dimethylamino-4'-N'-methyl-stilbazolium 2,4,6-trimethylbenzenesulfonate). Due to their extraordinarily high nonlinearities, small dielectric constants, and small dispersion from low to optical frequencies, the organic crystals are excellent materials for broadband THz generation.<sup>13,14</sup> They provide high laser to THz conversion efficiencies at room temperature, broad spectra, naturally collimated and aberration free THz beams,

and intrinsically carrier envelope (CEP) stable THz pulses.<sup>15</sup> A conversion efficiency of up to 3% with THz energies of 0.9 mJ<sup>16</sup> and a broad spectral content reaching 10 THz<sup>17</sup> were recently reported in the case of DSTMS crystals pumped at 1.25 and 1.5  $\mu\text{m}$ , respectively. Because of the beneficial phase matching conditions and high transparency in the near-IR, laser sources operating at the telecommunication wavelength of 1.5  $\mu\text{m}$  are commonly used as drivers for efficient THz generation in DAST.<sup>18,19</sup> However, because the absorption edge of DAST is situated at around 700 nm,<sup>20</sup> the crystal suffers from multi-photon absorption (MPA),<sup>21</sup> which acts on the saturation of the conversion efficiency, as well as on the crystal damage threshold, and restricts the applicable energy density of the driving pulses to a range of 20 mJ/cm<sup>2</sup>. In the case when a 200  $\mu\text{m}$  thick DAST crystal was pumped with 65 fs pulses, centered at 1.5  $\mu\text{m}$ ,<sup>21</sup> a drop in transmission by more than a factor of two (from more than 60% to less than 30%) at a pump energy density of 10 mJ/cm<sup>2</sup> (corresponding to the intensity of 0.15 TW/cm<sup>2</sup>) was monitored. Furthermore, MPA and subsequent free-carrier absorption of the THz radiation were identified to be responsible for the reduction of THz generated via OR.<sup>22</sup> Moreover, NL absorption can be a limiting factor for a low crystal damage threshold in EO crystals.<sup>23,24</sup>

In this work, we perform pioneering studies of THz generation in DAST driven by intense mid-IR pulses centered at 3.9 and 1.95  $\mu\text{m}$ . We validate that MPA in DAST can be suppressed to a large extent as compared to 1.5  $\mu\text{m}$  drivers, and no crystal damage can be observed for significantly higher pump energy densities (up to almost five times), pushing the generation efficiency to significantly higher limits. An unprecedented high optical-to-THz generation efficiency approaching 6% is observed in the case of a 1.95  $\mu\text{m}$  pump pulse.

## II. EXPERIMENTAL SETUP

To generate THz radiation by OR in a  $\sim 170 \mu\text{m}$  thick DAST crystal (Swiss Terahertz LLC), we use a high power mid-IR optical parametric chirped pulse amplifier (OPCPA),<sup>25,26</sup> operating at a repetition rate of 20 Hz and generating 30 mJ, 100 fs pulses centered at 3.9  $\mu\text{m}$ . The pulse duration and the chirp can be adjusted by tuning the distance between the gratings of the pulse compressor. Schematics of the THz generation setup and characterization of the driving pulses [performed with second harmonic generation (SHG) frequency resolved optical gating (FROG)] are shown in Fig. 1. Since the DAST crystal used in the experiments has a clear aperture of 6 mm, the beam diameter of the 3.9  $\mu\text{m}$  driving pulse is reduced by a telescope consisting of a pair of spherical mirrors to 3.2 mm at the FWHM level. To separate the THz radiation from the mid-IR driving pulse and to prevent saturation of the pyro-electric detector (THZ5I-BL-BNC, GenTec), several low pass filters (LPF) are used (see Fig. S1. of the [supplementary material](#) for details on the filter transmission). After filtering, THz pulses are steered to the diagnostic setup shown in Fig. 1(c).

Because our OPCPA is not continuously wavelength tunable, another infrared wavelength can be accessed by generating the second harmonics (SHs) at 1.95  $\mu\text{m}$  of the OPCPA output in a 100  $\mu\text{m}$  thick z-cut GaSe crystal [Fig. 1(b)]. During the SHG process, the temporal pulse profile cleans up as pulses shorten to 76 fs. After

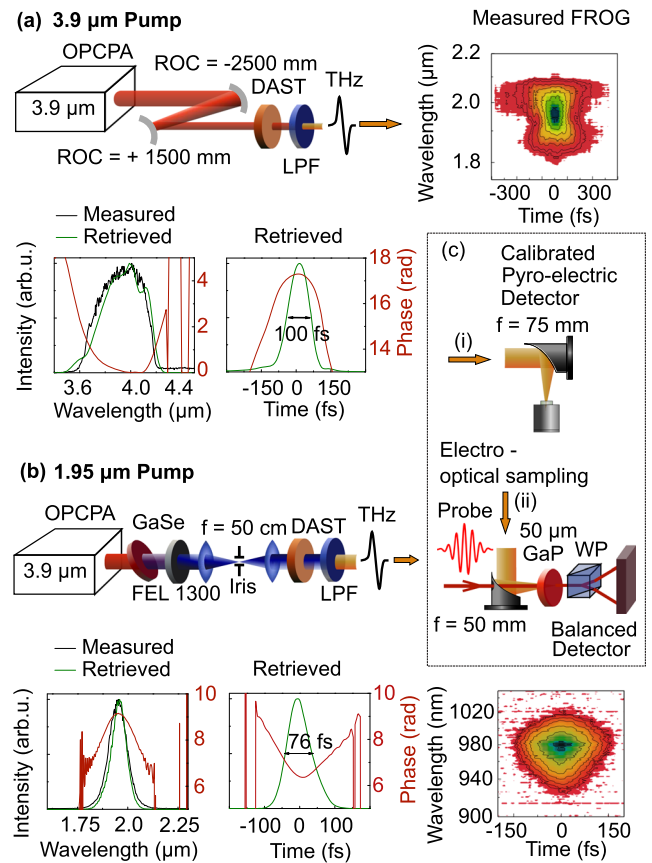


**FIG. 1.** Experimental setup and characterization of the driving 3.9  $\mu\text{m}$  (a) and 1.95  $\mu\text{m}$  (b) pulses. (c) Diagnostic setup for the THz-pulse characterization: (i) the THz energy is measured with a calibrated pyro-electric detector and (ii) the THz electric field is recorded by EOS in a 50  $\mu\text{m}$  thick GaP crystal. WP is the Wollaston prism.

SHG, fundamental pulses at 3.9  $\mu\text{m}$  are blocked by a long pass filter (FEL 1300, Thorlabs). In order to improve the SH beam quality, which is deteriorated because of the photo-induced inhomogeneity of the GaSe crystal,<sup>23</sup> spatial filtering of the generated SH is performed. The SH beam area on the DAST crystal is 1.4 mm<sup>2</sup>. The generated THz pulses are characterized by measuring the energy with a calibrated pyro-electric detector and by recording the THz electric field by electro-optical sampling (EOS) with a 50  $\mu\text{m}$  thick GaP crystal. 45-fs probe pulses for EOS are generated with a home built single stage non-collinear optical parametric amplifier (NOPA) operating at a central wavelength of 642 nm, which is synchronized with the mid-IR OPCPA system (the details are given in Fig. S3. of the [supplementary material](#)).

## III. RESULTS

### A. THz generation by 3.9 $\mu\text{m}$ driving pulses

We first examine THz generation with 3.9  $\mu\text{m}$  driving pulses, where the transmission of DAST drops to  $\sim 10\%$ .<sup>21</sup> Figure 2(a) depicts the mid-IR to THz conversion efficiency and generated THz

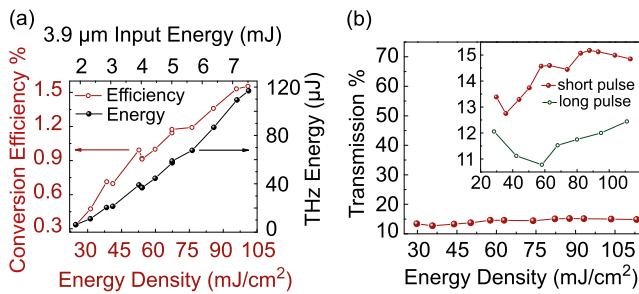


**FIG. 2.** (a) Optical-to-THz Conversion efficiency (red circles) and THz energy (black dots) in dependency of the energy density and input energy, respectively, for 3.9  $\mu\text{m}$  driving pulses. (b) Transmission of the 3.9  $\mu\text{m}$  pump pulse with respect to the pump fluence. The inset shows a magnified detail from 10.5% to 15.5%. Because the transmission slightly increases for higher pump energy densities (red dots), the experiment is repeated with long pulses stretched to more than 3 ps (green circles) to confirm features of NL photon bleaching.

pulse energy with respect to the pump fluence and pulse energy, respectively. Surprisingly, despite strong linear absorption, high conversion efficiencies of 1.5% and THz energies of up to 116  $\mu\text{J}$  can be achieved. When evaluating the THz pulse energies as well as the conversion efficiencies, we account for the transmission of the filters and 10 cm of air, through which the generated THz pulses propagate before reaching the pyro-electric detector. Taking the absorption of the crystal into account, the efficiency is commensurate or even superior as compared to conventional drivers at the telecommunication wavelength. In addition to phase-matching of the driving and generated THz fields, a necessary condition for high conversion efficiencies is a high second order NL susceptibility  $\chi^{(2)}$  of the crystal. In the case when the virtual energy levels of the parametric process are close to a real energy level, the NL susceptibility is considered to be resonantly enhanced.<sup>14</sup> Thus, one of the possible reasons for the high conversion efficiency is a resonant enhancement of the electro-optical coefficient in the vicinity of 3.9  $\mu\text{m}$ . Though, given that the complex permittivity of DAST at 3.9  $\mu\text{m}$  is actually unknown, we can only hypothesize about advantageous phase matching conditions and the enhanced electro-optical coefficient.

Nonetheless, the onset of saturation only appears at extraordinarily high pump fluences. Furthermore, despite the high linear absorption, optical damage cannot be observed for pump energy densities of 110  $\text{mJ}/\text{cm}^2$ , which can be attributed to a suppression of MPA. In order to verify this statement, we measure the dependence of the transmission of DAST on the pump fluence. As it can be seen in Fig. 2(b), when the crystal is pumped with compressed 100 fs pulses (red dots), the transmission, instead of decreasing, which is characteristic for MPA, even slightly increases at higher energy densities. This is a feature of NL photo-bleaching, wherein the leading edge of the pulse depletes the ground state of DAST. When the experiments are repeated with pulses stretched to a few ps (green dots), the transmission appears to be slightly lower and virtually independent on the pump fluence. Thus, we confirm that MPA of 3.9  $\mu\text{m}$  pulses does not occur at almost an order of magnitude higher pump intensities as compared to the case of 1.5  $\mu\text{m}$  pump pulses.<sup>21</sup>

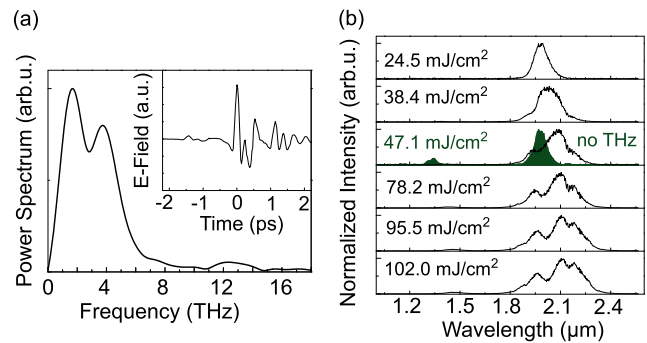


**FIG. 3.** (a) THz power spectrum measured with EOS in the case of 3.9  $\mu\text{m}$  driving pulses. The inset shows the temporal THz transient. (b) Spectra after propagation in DAST measured in the spectral range of 1100–2600 nm (corresponding to SHG of the pump pulse) for different pump fluences when the crystal is aligned for maximum THz generation. The green curve shows parts of the SH spectrum when the crystal is rotated such that THz generation is inhibited.

Finally, Fig. 3(a) shows the THz spectrum generated by 3.9  $\mu\text{m}$  pump pulses, measured with EOS. The experimental setup is purged with  $\text{N}_2$ , resulting in a reduced humidity of < 10%. The measurement reveals a multiple octave-spanning spectrum with a maximum at 2.1 THz, bandwidth of 4.2 THz FWHM, and spectral content extending up to 7.8 THz. The absolute electric field strengths can be obtained by measuring the THz pulse energy, spot size, and temporal field evolution. The THz beam radius at the  $1/e^2$  level is measured with the knife edge method (see Fig. S6 of the [supplementary material](#)) and accounts for  $w = 107 \mu\text{m}$ . Thus, the peak electric THz field can be estimated to be 40 MV/cm. The measured central frequency is similar to that for 1.5  $\mu\text{m}$  driving pulses reported in Ref. 19, wherein high optical-to-THz conversion efficiency of up to 2.2% are achieved but with only half the spectral bandwidth of 2 THz. The high conversion efficiency in Ref. 19 is ascribed to cascaded OR when a pump photon, after the emission of a THz photon, experiences a corresponding red shift and can again contribute to the generation of another THz photon, leading to multiple shifts of the initial pump spectrum toward longer wavelengths. Because a single optical photon of the pump pulse contributes to the generation of multiple THz photons, the Manley–Row limit is surpassed, i.e., the photon conversion efficiency, which is defined as the ratio between the number of THz and pump photons  $N(h\nu_{\text{THz}})/N(h\nu_p)$  can become substantially larger than 1. Although this process can initially result in higher optical-to-THz conversion efficiencies, it can also limit THz generation because the phase mismatch due to material dispersion with the newly generated photons (i.e., broader spectrum) can be enhanced.<sup>27</sup> In the case of 3.9  $\mu\text{m}$  driving pulses, the photon conversion efficiency is evaluated to be 0.56, which reveals minor, if any, contribution of cascaded effects for the THz generation process. An absence of cascaded OR is also supported by the fact that 3.9  $\mu\text{m}$  pulses, after propagation in DAST, do not experience any notable spectral broadening or other transformations dependent on the pump energy density (see Fig. S5 of the [supplementary material](#)). Linear absorption potentially could lead to a substantial local heating inside the crystal, which might affect THz generation and act on the optical damage threshold of the crystal.<sup>28,29</sup> In order to examine the effect of local heating, the experiments are

repeated at different repetition rates by reducing the repetition rate of the pump pulses with a mechanical chopper while keeping the pump fluence constant. Since no changes in the conversion efficiency, neither for the onset of saturation nor for the absolute values can be detected when reducing the repetition rate from 20 to 3 Hz, the linear absorption of DAST can be further ruled out as a possible limiting factor for THz generation at a 20 Hz repetition rate.

Because of the high second-order nonlinearity, aside from THz generation in DAST, SHG also takes place. SH spectra in the spectral range of 1100–2600 nm at different pump fluences are shown in Fig. 3(b) when the crystal is aligned for maximum THz generation. For higher pump energy densities, the spectrum of the generated SH continuously broadens to the red side. Modification of the SH spectrum takes place only when efficient THz generation is present. The spectrum shown by the green area in Fig. 3(b) is measured when the crystal axis is rotated (misaligned) to inhibit THz generation. It resembles the one measured at low-energy density when THz generation is rather inefficient. All of this gives a strong indication that an efficient nonlinear interaction between the generated SH and THz pulses takes place in the DAST crystal. On the other hand, the spectral content in the vicinity of  $2\ \mu\text{m}$  only accounts for  $\sim 1\%$  of the total pump energy. Hence, neither THz generation by SH (the details are given in III B) nor pump depletion of the  $3.9\ \mu\text{m}$  driving pulse due to SHG significantly influence the efficiency of THz generation. Note that, even for pump energy densities of more than  $100\ \text{mJ}/\text{cm}^2$ , saturation of the conversion efficiency cannot be distinctly observed.

## B. THz generation by $1.95\ \mu\text{m}$ driving pulses

In order to gain more information about THz generation in DAST when pumping at different wavelengths, experiments with  $1.95\ \mu\text{m}$  pulses are performed. Figure 4(a) depicts the transmission spectrum (black line) measured with a UV–Vis–NIR spectrophotometer (Cary 5G), revealing comparable transmission of  $\sim 60\%$  at  $1.5$  and  $1.95\ \mu\text{m}$ . Fresnel losses at the input and output surfaces of the crystal are not taken into account. However, the measurement of the transmission at different pump energy densities reveals that, despite a relatively small difference in wavelength, MPA is completely suppressed in the case of  $1.95\ \mu\text{m}$  pulses when the crystal is pumped with energy densities of up to  $80\ \text{mJ}/\text{cm}^2$ , corresponding to an intensity of  $\sim 1\ \text{TW}/\text{cm}^2$ . Mind that in the case of a  $1.5\ \mu\text{m}$  driver, more than 50% decrease in transmission due to MPA was observed at a ten times lower intensity ( $\sim 0.1\ \text{TW}/\text{cm}^2$ ).<sup>21</sup> Figure 4(b) shows the dependence of the THz conversion efficiency on the pump fluence when the crystal is pumped with  $1.95\ \mu\text{m}$  pulses. At the lowest pump fluence of  $7\ \text{mJ}/\text{cm}^2$ , an optical-to-THz conversion efficiency of  $\sim 2.4\%$  is evaluated. This is in good agreement with previously published values for shorter wavelength drivers. Conversion efficiency exceeding 2% could be achieved when a DAST crystal was pumped by a Cr:forsterite laser with a central wavelength of  $1.25\ \mu\text{m}$  and pump fluence around  $10\ \text{mJ}/\text{cm}^2$ ,<sup>18</sup> while Hauri *et al.*<sup>19</sup> demonstrated THz generation for  $1.2\text{--}1.5\ \mu\text{m}$  driving pulses in DAST with a wavelength independent efficiency of 2.2%. Similar results are reported for mosaic DSTMS<sup>16</sup> when the crystal is pumped with a  $1.25\ \mu\text{m}$  driver, wherein conversion efficiencies of more than 3% at a pump fluence of  $\sim 6.6\ \text{mJ}/\text{cm}^2$  are achieved, followed by a reduction of the efficiency for higher pump energy densities. Novelli *et al.*<sup>30</sup>

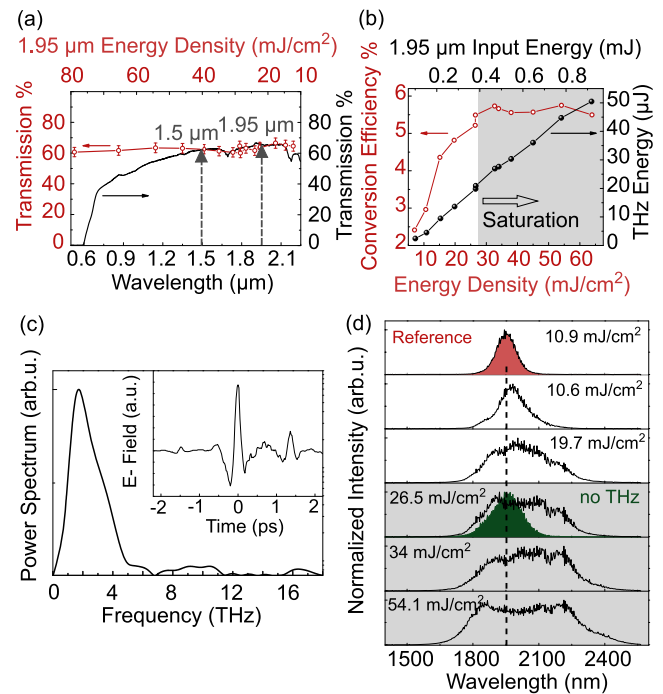


**FIG. 4.** (a) DAST transmission spectrum (black line) and dependence of the transmission at  $1.95\ \mu\text{m}$  on the pump fluence (red circles). (b) Optical-to-THz conversion efficiency (red circles) and THz pulse energy (black dots) in dependence of the energy density for  $1.95\ \mu\text{m}$  driving pulses. (c) THz power spectrum measured with EOS. The inset shows the temporal THz transient. (d) Pump spectra after propagation in DAST for different pump fluences when the EO crystal is optimized for maximum THz generation. The red filled area in the top panel shows a reference pump spectrum without the crystal. The spectrum measured when the crystal axis is rotated to inhibit THz generation is shown by the green area in the middle.

reported wavelength independent THz generation conversion efficiencies for  $1.5$  and  $2\ \mu\text{m}$  when DSTMS is pumped at a fluence of  $6.4\ \text{mJ}/\text{cm}^2$ . Thus, the THz conversion efficiency in the case of our  $1.95\ \mu\text{m}$  driving source is not surprising for low pump fluences since in addition to the commensurate transmission at  $1.5$  and  $1.95\ \mu\text{m}$ , DAST exhibits NL optical coefficients in the same order of magnitude for both wavelengths [ $d_{11}(1542\ \text{nm}) = 290$  and  $d_{11}(1907\ \text{nm}) = 210$ ].<sup>31</sup> A detailed calculation of the THz conversion efficiency with respect to phase matching conditions, coherence length, and the effective generation length is conducted in the [supplementary material](#), wherein we focus on a comparative study between driving pulses centered at  $1.5$  and  $1.95\ \mu\text{m}$ . However, in our case of  $1.95\ \mu\text{m}$  driving wavelength, the absence of MPA allows the application of substantially larger pump fluences up to  $30\ \text{mJ}/\text{cm}^2$  (compared to  $10\ \text{mJ}/\text{cm}^2$  for near-IR drivers) before the onset of saturation. Because the conversion efficiency scales linearly with respect to the pump fluence, this leads to exceptionally high THz conversion efficiencies of 5.7% and generated THz energies of  $50\ \mu\text{J}$ .

To further investigate the mechanism of this efficient THz generation, spectral transformations of pump pulses are monitored after propagation in DAST when the crystal is aligned for maximum THz generation. The spectrum at the top panel of Fig. 4(d) represents the

reference without the DAST crystal in the beam path. When the crystal is inserted into the beam, the spectrum slightly broadens at low pump fluences, which is a feature of self-phase modulation (SPM). With the further increase of the pump fluence, spectral broadening dominated on the red side of the spectrum gets increasingly pronounced and stabilizes at a pump fluence of about  $30 \text{ mJ/cm}^2$ , corresponding to the onset of saturation of the THz generation efficiency [Fig. 4(b)]. In contrast, when THz generation is inhibited, which is realized by rotating the crystal axis with respect to the polarization of the pump pulse, the spectrum exhibits a minor symmetrical spectral broadening that is ascribed to SPM [green filled area in Fig. 4(d)]. This observation strongly indicates cascaded OR, of which the presence is further confirmed by the power spectrum, measured with EOS [Fig. 4(c)]. The Fourier transformation reveals a maximum intensity at 1.7 THz with a spectral width of 2.6 THz FWHM and spectral components extending up to 5 THz. By taking this into account, we evaluate the photon conversion efficiency of more than 5, which implies cascaded OR. Next to the positive contribution to the conversion efficiency, cascaded OR results in a strong spectral broadening, which enhances phase mismatch, and can be identified as a possible limiting factor for efficient THz generation at higher pump fluences.<sup>27</sup>

#### IV. CONCLUSION

In conclusion, we demonstrated that suppression of MPA allows a shift in the onset of saturation of the optical-to-THz conversion efficiency for DAST to higher pump fluences by nearly an order of magnitude when the crystal is pumped with long wavelength driving sources as compared to  $1.5 \mu\text{m}$ . In the case of  $3.9 \mu\text{m}$  driving pulses, a conversion efficiency of 1.5%, similar to the case of conventional driving sources operating in the transparency region of DAST, was measured. Taking into account that more than 80% of the input energy is absorbed during propagation through the crystal, the effective conversion efficiency is even higher. As one of the possible reasons for the high efficiency and generated THz pulse energies, we propose a resonantly enhanced electro-optical coefficient. No indication for the influence of thermal effects on the THz generation or parasitic SHG is observed. In the case of  $1.95 \mu\text{m}$  driving pulses, record conversion efficiencies approaching 6% are determined. This beneficial outcome can be attributed to the capability of applying higher pump intensities as compared to  $1.5 \mu\text{m}$  and to cascaded OR. Cascaded OR is identified as both a mechanism through which a high conversion efficiency is achieved and a limiting factor for the THz generation efficiency when the newly generated spectral components promote a phase mismatch between the pump and THz pulses. These new insights of highly efficient THz generation in the vicinity of  $2 \mu\text{m}$  are very attractive in view of the recently developed Cr:ZnSe laser systems generating multi-mJ femtosecond pulses in the spectral range of  $2\text{--}2.5 \mu\text{m}$ .<sup>32</sup>

#### SUPPLEMENTARY MATERIAL

The [supplementary material](#) contains additional details about the experimental setup, filter and pulse characterization, detector calibration, and a comparative study on the coherence length for 1.95 and  $1.5 \mu\text{m}$  driving pulses.

#### ACKNOWLEDGMENTS

This work was supported by Österreichische Forschungsförderungsgesellschaft (Grant No. 867822 HABRIA), Hochschuljubiliäumsfond der Stadt Wien (Grant No. H-260733/2020), and the Austrian Science Fund (Grant Nos. 27577-N27 and I4566-N).

#### DATA AVAILABILITY

The data that support the findings of this study are available within the article and its [supplementary material](#).

#### REFERENCES

- <sup>1</sup>M. Tonouchi, *Nat. Photonics* **1**, 97 (2007).
- <sup>2</sup>P. U. Jepsen, D. G. Cooke, and M. Koch, *Laser Photonics Rev.* **5**, 124 (2011).
- <sup>3</sup>J. B. Baxter and G. W. Guglietta, *Anal. Chem.* **83**, 4342 (2011).
- <sup>4</sup>B. H. Kolner, R. A. Buckles, P. M. Conklin, and R. P. Scott, *IEEE J. Sel. Top. Quantum Electron.* **14**, 505 (2008).
- <sup>5</sup>A. I. McIntosh, B. Yang, S. M. Goldup, M. Watkinson, and R. S. Donnan, *Chem. Soc. Rev.* **41**, 2072 (2012).
- <sup>6</sup>O. Schubert, M. Hohenleutner, F. Langer, B. Urbanek, C. Lange, U. Huttner, D. Golde, T. Meier, M. Kira, S. W. Koch, and R. Huber, *Nat. Photonics* **8**, 119 (2014).
- <sup>7</sup>C. Kübler, H. Ehrke, R. Huber, R. Lopez, A. Halabica, R. F. Haglund, and A. Leitenstorfer, *Phys. Rev. Lett.* **99**, 116401 (2007).
- <sup>8</sup>T. Kampfrath, K. Tanaka, and K. A. Nelson, *Nat. Photonics* **7**, 680 (2013).
- <sup>9</sup>P. Salén, M. Basini, S. Bonetti, J. Hebling, M. Krasilnikov, A. Y. Nikitin, G. Shamuilov, Z. Tibai, V. Zhaunerchyk, and V. Goryashko, *Phys. Rep.* **836–837**, 1 (2019).
- <sup>10</sup>M. A. Sentef, A. F. Kemper, A. Georges, and C. Kollath, *Phys. Rev. B* **93**, 144506 (2016).
- <sup>11</sup>T. Qi, Y.-H. Shin, K.-L. Yeh, K. A. Nelson, and A. M. Rappe, *Phys. Rev. Lett.* **102**, 247603 (2009).
- <sup>12</sup>S. Baierl, M. Hohenleutner, T. Kampfrath, A. K. Zvezdin, A. V. Kimel, R. Huber, and R. V. Mikhaylovskiy, *Nat. Photonics* **10**, 715 (2016).
- <sup>13</sup>M. Jazbinsek, L. Mutter, and P. Gunter, *IEEE J. Sel. Top. Quantum Electron.* **14**, 1298 (2008).
- <sup>14</sup>M. Jazbinsek, U. Puc, A. Abina, and A. Zidansek, *Appl. Sci.* **9**, 882 (2019).
- <sup>15</sup>C. Vicario, B. Monozslai, and C. P. Hauri, *Phys. Rev. Lett.* **112**, 213901 (2014).
- <sup>16</sup>C. Vicario, A. V. Ovchinnikov, S. I. Ashitkov, M. B. Agranat, V. E. Fortov, and C. P. Hauri, *Opt. Lett.* **39**, 6632 (2014).
- <sup>17</sup>M. Shalaby and C. P. Hauri, *Nat. Commun.* **6**, 5976 (2015).
- <sup>18</sup>C. Vicario, M. Jazbinsek, A. V. Ovchinnikov, O. V. Chefonov, S. I. Ashitkov, M. B. Agranat, and C. P. Hauri, *Opt. Express* **23**, 4573 (2015).
- <sup>19</sup>C. P. Hauri, C. Ruchert, C. Vicario, and F. Ardana, *Appl. Phys. Lett.* **99**, 161116 (2011).
- <sup>20</sup>L. Cao, B. Teng, D. Xu, H. Zhao, L. Hao, J. Yao, and J. Guo, *RSC Adv.* **6**, 101389 (2016).
- <sup>21</sup>C. Vicario, B. Monozslai, G. Arisholm, and C. P. Hauri, *J. Opt.* **17**, 094005 (2015).
- <sup>22</sup>Z. Zhen-Yu, H. Sophie, and T. Jérôme, *Chin. Phys. Lett.* **25**, 1868 (2008).
- <sup>23</sup>J. Guo, J.-J. Xie, L. Zhang, F. Chen, K. Jiang, S. V. Alexeev, Y. M. Andreev, K. A. Kokh, G. V. Lanskiy, V. F. Losev, D. M. Lubenko, A. V. Shaiduko, and V. A. Svetlichnyi, in *XIX International Symposium on High-Power Laser Systems and Applications 2012*, edited by K. R. Allakhverdiev (International Society for Optics and Photonics, SPIE, 2013), Vol. 8677, pp. 359–366.
- <sup>24</sup>Z.-S. Feng, Z.-H. Kang, X.-M. Li, Z.-B. Wang, J.-Y. Gao, Y. M. Andreev, V. V. Atuchin, K. A. Kokh, G. V. Lanskiy, A. I. Potekae, A. V. Shaiduko, and V. A. Svetlichnyi, *AIP Adv.* **4**, 037104 (2014).

- <sup>25</sup>G. Andriukaitis, T. Balčiūnas, S. Ališauskas, A. Pugžlys, A. Baltuška, T. Popmintchev, M.-C. Chen, M. M. Murnane, and H. C. Kapteyn, *Opt. Lett.* **36**, 2755 (2011).
- <sup>26</sup>V. Shumakova, S. Ališauskas, P. Malevich, C. Gollner, A. Baltuška, D. Kartashov, A. M. Zheltikov, A. V. Mitrofanov, A. A. Voronin, D. A. Sidorov-Biryukov, and A. Pugžlys, *Opt. Lett.* **43**, 2185 (2018).
- <sup>27</sup>K. Ravi, W. R. Huang, S. Carbajo, X. Wu, and F. Kärtner, *Opt. Express* **22**, 20239 (2014).
- <sup>28</sup>M. Shalaby and C. P. Hauri, *Sci. Rep.* **5**, 8059 (2015).
- <sup>29</sup>T. Matsukawa, K. Nawata, T. Notake, F. Qi, H. Kawamata, and H. Minamide, *Appl. Phys. Lett.* **103**, 023302 (2013).
- <sup>30</sup>F. Novelli, B. Guchhait, and M. Havenith, *Materials* **13**, 1311 (2020).
- <sup>31</sup>L. R. Dalton, P. Günter, M. Jazbinsek, O.-P. Kwon, and P. A. Sullivan, *Organic Electro-Optics and Photonics: Molecules, Polymers, and Crystals* (Cambridge University Press, 2015).
- <sup>32</sup>X. Ren, L. H. Mach, Y. Yin, Y. Wang, and Z. Chang, *Opt. Lett.* **43**, 3381 (2018).